Exciton Dynamics in FMO Bacteriochlorophyll Protein at Low Temperatures

ARTICLE *in* THE JOURNAL OF PHYSICAL CHEMISTRY B · FEBRUARY 1997

Impact Factor: 3.3 · DOI: 10.1021/jp9633761 · Source: PubMed

Exciton Dynamics in FMO Bacteriochlorophyll Protein at Low Temperatures

Arvi Freiberg,*,†,‡ Su Lin,‡ Kõu Timpmann,† and Robert E. Blankenship‡

Institute of Physics, EE2400 Tartu, Estonia, and Department of Chemistry and Biochemistry and Center for the Study of Early Events in Photosynthesis, Arizona State University, Tempe, Arizona 85287

Received: October 29, 1996; In Final Form: February 14, 1997[⊗]

A time response over almost 5 decades (from 10^{-13} to about 10^{-8} s) to a (sub)picosecond laser pulse excitation has been observed in the Fenna, Matthews, and Olson (FMO) antenna protein trimer. The FMO protein is unique in having a fine-structured bacteriochlorophyll *a* Q_y exciton absorption spectrum over the whole investigated temperature range between 6 and 160 K. As measured by a two-color pump−probe differential absorption, the population decay of the exciton states of seven strongly coupled bacteriochlorophyll *a* molecules in a protein monomer is the dominant dynamical process in the subpicosecond time domain. The through-band scattering takes a few picoseconds and depends only weakly on temperature, probably because of a low density of exciton states. At low temperatures, evidence for a slow pico−nanosecond relaxation process has also been obtained via time-dependent red-shift and broadening of the exciton emission spectrum. Two nonexclusive tentative interpretations to this effect have been provided. The phenomenon may be due to exciton solvation in the surrounding protein and water−glycerol matrix or/and due to slow scattering of closely spaced bacteriochlorophyll *a* exciton states in a protein trimer. The shape of the excited-state absorption spectrum (arising from transitions between singly and doubly excited exciton states) and its oscillator strength has been roughly estimated from the analysis of the pump−probe spectrum. The spectrum peaks at around 805 nm and is less featured compared to the ground-state absorption spectrum. Both spectra have comparable strength.

1. Introduction

Various pigment−protein complexes in the photosynthetic apparatus function to carry out highly efficient light energy harvesting, transfer and conservation. The nature of pigment excitations, the energy-transfer mechanism, and the exact role of the protein moiety in these pigment−protein complexes are still under debate. The available structural data evidence about very dense packing of pigments in antenna proteins that makes possible a strong resonant coupling between the pigments and formation of collective excited electronic states, excitons. The protein provides a rigid framework to fix the pigments in certain (favorable) positions. Via dispersive and other interactions, it also regulates the energetics of the pigments. Excitons may encompass the whole physical size of the pigment aggregate or just a part of it, depending on time, the excitonic coupling strength, and on various perturbations set by the environment. For the latter temperature is an essential parameter. However, very little is known about the dynamics of pigment−pigment and pigment−protein interactions. At the same time, knowledge of how energy is directed along specific channels in a protein or is dissipated into heat is important for understanding of the functioning of all (not only photosynthetic) proteins. Energy relaxation in spatially confined molecular structures has currently also a more general interest connected with the problems of molecular electronics and molecular mechanics.

In this work, we study the relaxation dynamics of light excitations in a bacteriochlorophyll *a*-protein complex called the FMO protein (after the names of the pioneer investigators Fenna, Matthews, and Olson).

In the green sulfur photosynthetic bacteria, the FMO proteins play a double role: as an antenna for collecting the light energy and as a mediator of light excitations between the extra-membrane chlorosome antenna and the cell membrane (for a recent review, see ref 1). The FMO protein consists of three identical subunits, each enclosing seven closely but irregularly spaced bacteriochlorophyll *a* (BChl) molecules. The absorption spectrum of the FMO protein at low temperatures (≤150 K) reveals a multiline structure in the 800−830 nm region unique among other pigment−proteins. This has been interpreted as due to strong resonance coupling between the BChl molecules, predominantly within the same monomer subunit.[2−4]

Two different techniques, two-color femtosecond time-resolved differential absorption (pump−probe) spectrometry and picosecond time-resolved spontaneous emission spectroscopy, have been used in this work to study the dynamics of excitons in the FMO proteins. The two techniques give complementary information that a single method alone is not able to provide.

For example, the pump−probe technique renders a unique time resolution limited only by the laser pulse width and an opportunity to study the optical transitions from the directly pumped excited electronic states to the higher ones. At the same time, the pump−probe spectroscopy data are difficult to interpret because the differential spectrum is a mixture of the ground-state absorption, excited-state absorption, and stimulated emission contributions, of which at least the last two are time dependent. The method has also a relatively low sensitivity. The fluorescence emission technique enjoys an excellent sensitivity, and the data are relatively straightforward to interpret. However, this method usually has a rather poor detector-limited time resolution. Investigations have been performed in a wide range of temperatures (between 6 and 160 K (fluorescence emission) and between 15 and 160 K (pump−probe)) in order to take advantage of the exciton structure by choosing excitation wavelengths close to the distinct exciton absorption bands and to study the influence of temperature to the energy relaxation processes. Preliminary data of this study have been presented.[5−8]

Ultrafast energy transfer and spectral equilibration phases in the 0.1−2 ps time range have recently been found in these proteins at room temperature.[9, 10] Because of the structureless spectra, the assignment of the deduced kinetic constants to

† Institute of Physics.
‡ Arizona State University.
⊗ Abstract published in *Advance ACS Abstracts,* August 1, 1997.

S1089-5647(96)03376-7 CCC: $14.00

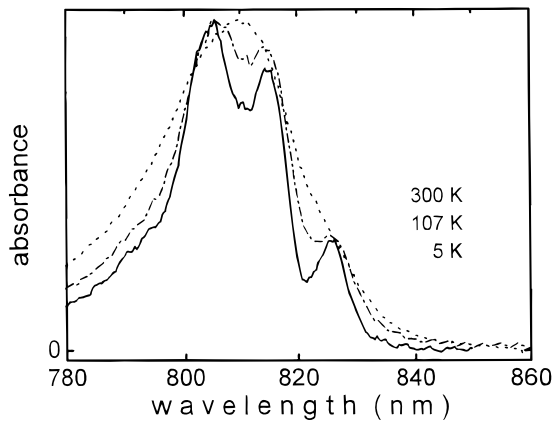

Figure 1. Steady-state absorption spectra of FMO proteins at 5 K (solid curve), 107 K (dash−dotted curve), and 300 K (dotted curve).

specific processes was difficult. Earlier laser spectroscopic studies of FMO proteins at low temperatures, relevant to this work, include hole-burning[11] and picosecond time-resolved accumulated photon echo[11] techniques. During the writing of this article, we learned of new 19 K data from the Struve's group[13,14] by utilizing a high repetition rate femtosecond pump−probe setup.

The rest of the paper is organized as follows. In section 2, the experimental techniques and the measurement conditions are detailed. Special attention was paid to avoid too high excitation intensities during femtosecond differential absorption experiments. Section 3 presents the results of the time-resolved measurements as a function of pump wavelength and temperature. Section 4 deals with the evaluation and interpretation of the data. Section 5 contains concluding remarks.

2. Experimental Section

2.1. Samples and Handling. The FMO trimers were isolated from the green sulfur bacterium *Chlorobium tepidum* as described in refs 9 and 15. The protein solution in the 20 mM Tris-HCl buffer (pH = 8.0) was diluted with glycerol in a 1:2 volume ratio, fixed between two fused quartz plates about 1.2 mm apart, and slowly cooled in a temperature-controlled cryostat (Air Products, USA, or UTREKS, Ukraine). The optical density of the samples was checked by the room-temperature absorption maximum at 808 nm (Figure 1). Samples with optical density around 0.2 or between 0.8 and 1.3 were used in the fluorescence emission and pump−probe measurements, respectively. At low temperatures, the absorption maximum shifts to about 805 nm, but its optical density remains almost the same.

The optical quality of the samples at low temperatures is a concern in the pump−probe approach because of severe cracking of the sample upon cooling below 130−140 K that results in a strong scattering of the laser beams. This problem was overcome by coating the inner surfaces of the quartz plates with Repel−Silane (a solution of dimethyldichlorosilane in trichloroethane). Only a few cracks were then observed over the 4 cm^2 sample surface area.

2.2. Femtosecond Pump−Probe Experiments. The femtosecond transient absorption spectrometer of the Center for the Study of Early Events in Photosynthesis of the Arizona State University used in these experiments has been described in more detail earlier.[16,17] The 70 ps pulses from the mode-locked Nd:YAG laser were compressed in a fiber compressor, frequency doubled, and then used to pump a rhodamine 6G dye laser (Spectra Physics). The output pulses from the dye laser at 590 nm were further compressed and then amplified in a regenerative amplifier (Continuum) operating at 540 Hz. Amplified pulses with pulse energy about 200 μJ were split into two parts. One portion was used to form a pump beam, either directly (at 590 nm) or via generation of a spectral continuum in a 1.2 cm rotating quartz plate (for the 790−830 nm region). Narrow band-pass (5 nm) interference filters were used to select the needed excitation wavelengths out from the continuum. Fine-tuning was achieved by tilting the filters in the laser beam. Excitation pulses were then reamplified by a prism dye amplifier (Santa Ana) pumped by the regenerative amplifier. The other portion was used to generate a spectral continuum in a 1 cm flowing water cell from which the probe and reference beams were formed. The variable time delay of the probe and reference beams relative to the pump beam was provided by a computer-controlled translation stage. The sample transmission spectra at probe (p) and reference (r) channels, $T_{p,r}(\lambda,t)$, were analyzed by a spectrograph equipped with a dual-array optical multichannel detector (Princeton Instruments). The optical density (absorbance) spectra at different time delays, δt, were then calculated as

$$OD(\lambda,t) = \log(T_r/T_p) \quad (1)$$

The time-resolved absorption difference spectrum is defined as the difference between optical density spectra of the sample perturbed by the pump pulse and of the unperturbed sample.

The sensitivity limit of the spectrometer for the kinetics measurements is few times 10^{-3} OD units. To get an acceptable signal-to-noise ratio, at each time delay the result of 2160 laser shots was collected and averaged. Each scan is divided to 100 points. Up to 10 different scans were measured and averaged at minimal used pump pulse intensity about 50 $\mu J/cm^2$ (corresponding to about 1.3×10^{14} absorbed quanta/cm^2 at 805 nm). The probe pulse intensity per spectral unit was maintained several orders of magnitude less than the pump pulse intensity. Different scanning lengths from 1.35 ps to about 1100 ps were probed in order to get an overview of various relaxation phases. In most cases, however, two time scales, 10 and 100 ps, were exploited. The pump and probe beam polarizations were always at the "magic angle", 54.7°. The pump pulse duration measured at the sample position was about 150 fs. The spectra were measured with 0.5 or 1.0 nm steps between data points.

Assuming the ground-state absorption cross section of the FMO protein trimer of 1.8×10^{-15} cm^2 and the one OD unit sample optical density, roughly 1 trimer out of 4.3 trimers (or 1 protein monomer out of about 13 monomers, each of them including 7 Bchl molecules) is getting excited at the minimal pump pulse intensity. This estimate is based on the ground-state absorption cross section 2.3×10^{-16} cm^2 of the BChl molecule[18] and on the results of the exciton absorption cross section calculations in FMO proteins.[3,4] No significant changes of the spectral and temporal behavior in the subpicosecond and picosecond time range were observed when checking with several times more intense pump pulses. This indicates that our data should not be distorted by multiple excitation effects, such as singlet−singlet annihilation.

In ref 19 where the problem of singlet−singlet annihilation in FMO complexes was specifically addressed, it was shown that the annihilation occurs only in the trimers in which more than one excitation is created by a pump pulse. According to the Poisson distribution, the probability to have n excitations in a trimer is

$$p(n) = (S^n/n!)\exp(-S) \quad (2)$$

where S is the average trimer excitation probability. At the above intensity, $S = 0.23$ and the probability to find simultaneously two excitiations in a trimer is a mere 2%. Furthermore,

according to ref 19, the characteristic singlet−singlet annihilation time is 7 ps at both room temperature and 77 K and is governed by the intermonomer energy transfer. As the Q_y exciton scattering takes only a couple of picoseconds (see section 3), the annihilation is basically related to the thermalized exciton distribution and cannot essentially interfere with the exciton relaxation process which is the main interest of the pump−probe study.

Accumulation of excitons in the triplet states and following annihilation of the singlet and triplet excitons[20] should not be a concern also in this low repetition-rate experiment because of the relatively short triplet lifetime (55 μs[20]) compared to the 1.85 ms time interval between successive pump pulses.

2.3. Picosecond Fluorescence Emission Experiments. The picosecond emission spectrometer (picosecond spectrochronograph) of the Institute of Physics in Tartu has been described in ref 21. In the present version, it consists of a Coherent 700 styril-9M mode-locked dye laser synchronously pumped at 76 MHz by a Coherent Antares 76S Nd:YAG laser as an excitation source with a 3−5 ps pulse width, a subtractive-dispersion double-grating monochromator (LOMO, Russian Federation) as a spectral analyzer, and a Hamamatsu C1587 temporal photometer synchroscan streak camera as a fast detector. The streak camera was linked via a vidicon to an OSA 500 optical spectrum analyzer (B&M Spektronik, FRG). The scattering from the sample at excitation wavelength was repeatedly recorded and used as an instrument response function. The typical instrument response function fwhm during these measurements was 12−15 ps. The spectral slit width was 2 nm. No degradation of the samples or nonlinear excitation effects was observed at the used average excitation light intensities $\leq$0.15 W/cm^{-1}.

Steady-state absorption and fluorescence emission spectra were measured by conventional means.

2.4. Data Analysis. Global as well as simple one-band analysis of the kinetics has been performed. Lifetimes were calculated using a least-squares fitting algorithm assuming multiexponential kinetics and taking into account the finite instrument response function. The time resolved absorption, ΔOD(λ,t), or fluorescence emission, $I(\lambda,t)$, spectra were built as

$$\Delta\mathrm{OD}(\lambda,t) = I(\lambda,t) = \Sigma \mathrm{A}_i(\lambda)\exp(-t/\tau_i) \qquad (3)$$

where the sum was over the number of kinetic components used in the fitting procedure. A plot of A_i versus wavelength, called a decay-associated spectrum (DAS), represents the amplitude of the ith kinetic component with time constant τ_i. The peak energies and bandwidths of the time-resolved emission spectrum were obtained by fitting to Gaussian band shapes.

3. Results

3.1. Femtosecond Pump−Probe Data. *3.1.1. Spectra and Kinetics at 15 K Excited at the Maximum of the Q_y Exciton Band.* Figure 2 shows time-resolved spectra (TRS) excited at 803 nm. For clarity, here and below the TRS probed with a light continuum at different picosecond delay times between the pump and probe pulses are offset vertically to avoid overlapping. Notice that the time delays in Figure 2 are fixed relative to an arbitrary time "zero". In the used 100 ps long scan case, the time "zero" was determined with about 1 ps precision, i.e., to get the proper time delay, one has to add about 1 ps to the numbers given in Figure 2. Prompt bleaching over the whole Q_y ground-state absorption spectrum region is observed at small delays, consistent with its exciton origin. Around 795 nm, also a weak net positive amplitude signal appears. The dominant

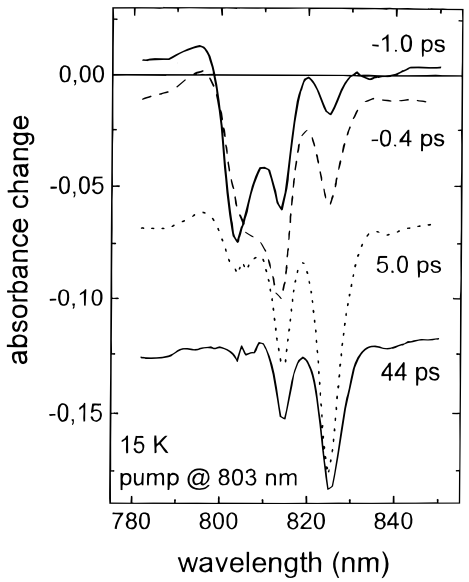

Figure 2. Isotropic pump−probe spectra at several probe pulse time delays. Note that the proper time "zero" is at about −1 ps (see text). Excitation is at 803 nm with 5 nm bandwidth and about 150 fs long pulses. Temperature is 15 K, spectral resolution is 1 nm per point.

effect at later times is a redistribution of the spectral intensity in favor of longer wavelengths. The spectral redistribution is accompanied by a small (up to 1.5 nm) dynamic red-shift of the longest wavelength band to 826 nm in about 20 ps. This Stokes shift may be a manifestation of a spectral inhomogeneity, slow exciton relaxation within the 825 nm band, and/or protein matrix perturbations by excitations in the BChl aggregate (see the discussion in section 4). The small band-shift of the differential absorption spectra correlates with the small net Stokes shift between the steady-state absorption and fluorescence spectra.[6]

At probe pulse delays, t, long compared to the pulse width when the coherent coupling effects are negligible, the TRS contains contributions from bleaching of the ground-state absorption (cross section, σ_{GB}), stimulated emission from the excited state (σ_{SE}), and absorption from one-exciton to two-exciton states (σ_{ESA}):[18,22]

$$\Delta\mathrm{OD}(\lambda,t) = [\sigma_{ESA}(\lambda,t) - \sigma_{GB}(\lambda,t) - \sigma_{SE}(\lambda,t)]n(t)d \qquad (4)$$

Here $n(t)$ is the concentration of excited molecules at time t and d is the optical path length. Since, like in our case, the spectral width of the pump pulse is comparable to the width of the inhomogeneous distribution function of ground-state transition energies (ground-state absorption bandwidth), the transient hole-burning effect in the ground-state population[23] is weak and the ground-state bleaching (GB) spectrum, $\sigma_{GB}(\lambda,t)$, can be considered constant in time. The time evolution of TRS at short times compared with the excited-state lifetime (the $n(t)$ term in eq 4) is then governed by the changing contributions of stimulated emission (SE) and excited-state absorption (ESA) spectra into the ΔOD(λ,t) in the course of the population relaxation of exciton states.

According to eq 4, the TRS in Figure 2 are dominated by the GB and SE contributions. The positive amplitude band around 795 nm at short times must be due to ESA. The evolution of the TRS reflects ultrafast loss of population of the initially prepared exciton states and simultaneous gain of population of the lower-energy states. Notably, the structure of the TRS at long times is more clear-cut than the structure of the ground-state absorption spectrum or of the TRS at early

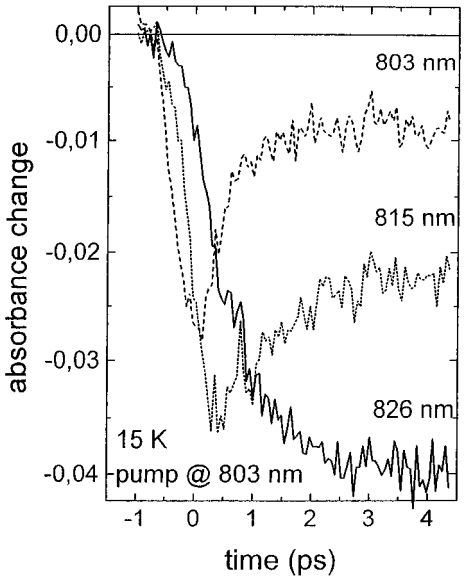

Figure 3. Short-time absorbance kinetics detected close to the band peaks of the ground-state absorption spectrum. Excitation is at 803 nm, temperature is 15 K.

times. This is because the ESA enters into eq 4 with different sign compared to the two other contributions (GB and SE) and evidently compensates the unstructured pedestal of the last. A weak side band around 839 nm is wholly due to SE, as a comparison with the steady-state fluorescence spectrum (see discussion below and ref 6) proves.

The relaxation kinetics at different probe wavelengths around the three major peaks in the differential absorption spectra is demonstrated in Figure 3. The kinetics at all probe wavelengths are complex and cannot be represented by a single-exponential decay. The decay of the initially prepared exciton state is ultrafast and takes not more than a few hundred femtoseconds. The band at 815 nm gains intensity within about half a picosecond and decays in about 1−2 ps. Only a few picoseconds are needed for the population of the lowest exciton state to reach its maximum.

The described behavior is what one would expect in the case of the sequential relaxation of the initial exciton population down an energetic ladder of exciton states. These qualitative conclusions were confirmed by the global analysis that revealed as a minimum three kinetic constants (the number of constants is limited by the available signal-to-noise ratio) needed to fit the kinetics simultaneously over a broad spectral range (Figure 4). The two shortest constants of 0.25 ± 0.15 ps and of 1.0 ± 0.2 ps with a characteristic wavelength-dependent sign of their amplitudes can be assigned to the interexciton relaxation time constants. The long 150 ps decay constant spreading over the whole spectrum and having a negative amplitude can be assigned to the excited-state lifetime.

It should, however, be pointed out that this relaxation scheme is only a rather crude model of a real behavior. This is made clear by examining Figure 5 together with Figure 4. Figure 5a demonstrates a wavelength-dependent decay at around the lowest energy exciton band, whereas the global analysis revealed only one decay component in this region. The decay at the red edge of the 826 nm band is the slowest, but clearly still not single-exponential. In the two-exponential approximation one has 16 and 110−150 ps decay components. This is also true in the 815 nm region (Figure 5b). The kinetics are fit best, if besides the dominant 1 ps decay component, a contribution of several slower ones of varying amplitudes is assumed. On the 500 ps scale the decay of the 815 nm band looks very much

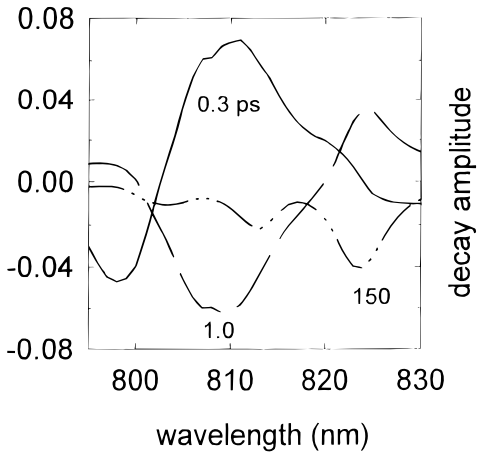

Figure 4. Decay associated spectra at 15 K from the global analysis of absorbance kinetics. Excitation is at 803 nm, temperature is 15 K. Indicated are corresponding decay constants in picoseconds.

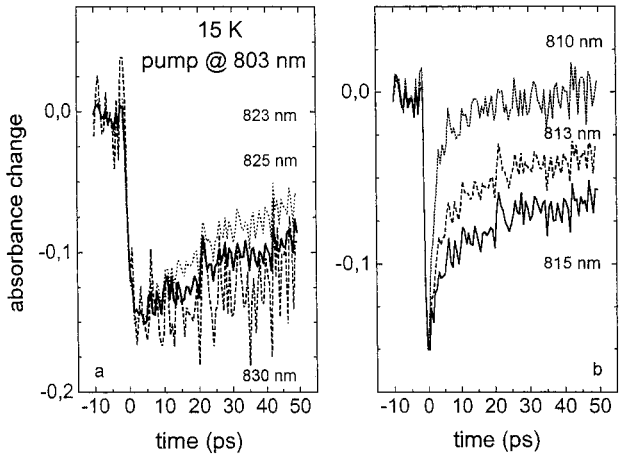

Figure 5. Normalized absorbance kinetics at different probe wavelengths close to the band peaks at 826 (a) and 815 nm (b). Excitation is at 803 nm; temperature is 15 K.

like the decay of the 826 nm band. The more spread out structure of the decay associated spectra (DAS) in Figure 4 compared to the TRS in Figure 2 evidently points to these difficulties with data analyses, caused by limited signal-to-noise ratio.

The ESA signal around 795 nm (Figure 6a) appears with about 0.3 ps delay and decreases all but with the 1.3 ± 0.2 ps decays constant. A longer time scale, as in Figure 6b, reveals additional components with 17 and 111 ps decay. These data compared with the decay kinetics of the 815 nm band provide good evidence that the main contribution to the ESA at 795 nm give the one-exciton to two-exciton transitions starting from the one-exciton band center around 815 nm.

3.1.2. Dependence on Pump Wavelength. The pump wavelength selects the kinetic energy that excitons will initially have. Besides the already described 803 nm excitation, four other pump wavelengths creating excitons with different energy either in the Q_y band (at 790, 815, and 832 nm) or in the upper Q_x band (at 590 nm) were used.

The 790 and 803 nm excitations produce rather similar results. There are some minor variations in the dynamics that, however, are very difficult to rationalize due to mingled kinetics. Pumping at 815 nm results in a strong resonant bleaching at zero time due to SE. At later times, both the relative amplitudes of the TRS bands and their evolution are again fairly similar to the 803 nm pump case. In the case of excitation at the red edge of the absorption band at 832 nm one would not expect

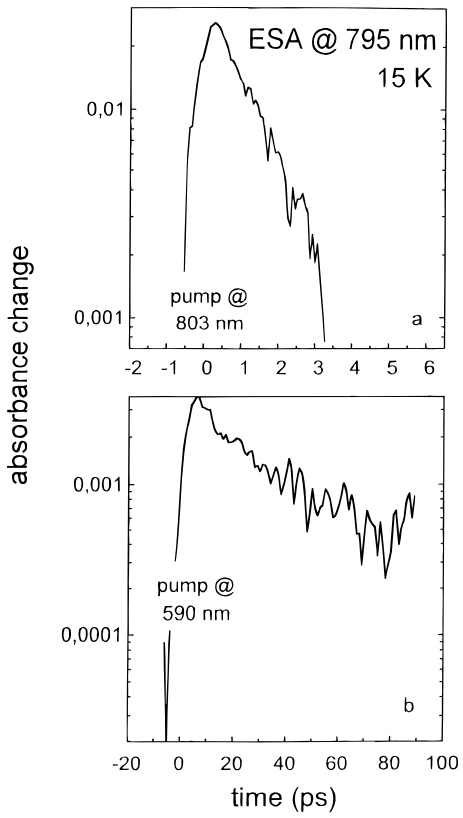

Figure 6. ESA kinetics measured at 795 nm in the case of two different excitation wavelengths: 803 (a) and 590 nm (b). Note different time axes used for the parts (a) and (b) and a logarithmic absorbance scale. Temperature is 15 K.

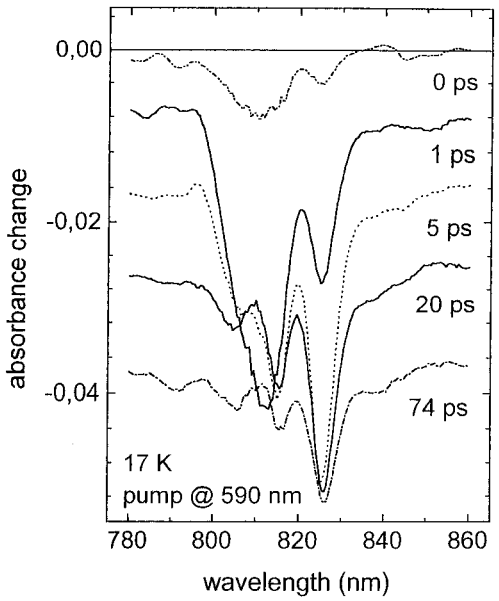

Figure 7. Pump−probe spectra excited at 590 nm. Spectral step is 0.5 nm per point. Temperature is 17 K.

any time evolution of the differential absorptium spectrum. This prediction was confirmed by the experiment (data not shown).

The TRS at the high-energy 590 nm excitation are shown in Figure 7. Although the responses are generally similar, there are few notable differences when Figure 7 is compared with Figure 2 at 803 nm excitation. In Figure 7, only a single unstructured and broad bleaching band in the 805−815 nm region is seen at early times (0−3 ps), whereas in Figure 2, the two subbands (at about 805 and 815 nm) are clearly distinguishable at all times. The familiar three-band structure with peaks

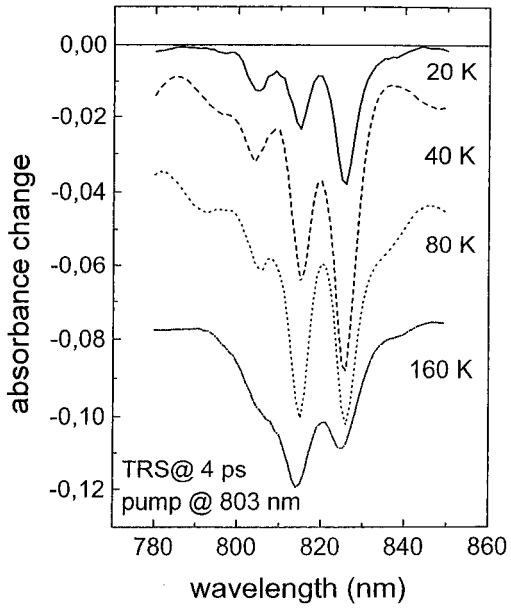

Figure 8. Pump−probe spectra at different temperatures, recorded 4 ps past excitation pulse at 803 nm.

at 805, 815, and 826 nm appears at later times also in the case of 590 nm excitation. After 5 ps when the intraband exciton relaxation is essentially terminated, the relative amplitudes of the 815 and 805 nm bands are almost independent of the pump wavelength. Note again the dynamic red-shift of the lowest energy band apparent at longer delay times.

The confused spectral structure immediately after the pump pulse at 590 nm may, in principle, be caused by temporal heating of the Bchl aggregate as a result of ultrafast dissipation of the 4830 cm^{-1} energy during the $Q_x \Rightarrow Q_y$ internal conversion process. However, the unbroadened 826 nm band in the same TRS seems not to support this version. Therefore, the effect was assigned to almost simultaneous and nonselective population of all the states in the Q_y exciton band via internal conversion. Overlapping of the ESA and SE spectral contours from different populated states apparently lead to the observed loss of fine structure of the TRS at early times. The global analysis indeed revealed a 0.3 ps rise time of the signal over the whole TRS spectrum, probably due to internal conversion.

3.1.3. Dependence on Temperature. The influence of temperature on TRS at 4 ps is shown in Figure 8. The most prominent spectral changes observed by increasing temperature are loss of some fine structure and an increased amplitude of the 815 nm band. These are rather obvious consequences of the thermally induced broadening of the ground-state absorption spectrum (compare with Figure 1) and of increased equilibrium population of the upper exciton states, clearly observable in the steady-state fluorescence spectra.[6,15]

As the kinetics in Figure 9 testify, the exciton relaxation pattern and even the relaxation rate is notably insensitive to temperature. Global analysis invariably gives three dominant kinetic constants. The two shorter constants (about 0.3 and about 1 ps) characterize the exciton equilibration phases. The longest one is determined by the exciton lifetime. Yet, a closer look of Figure 9 reveals some characteristic trends. First, there is a slight acceleration of relaxation when temperature is increased from 20 to 80 K. At still higher temperatures the relaxation seems to slow again. Note that the exciton dephasing processes are much more sensitive to temperature. An order of magnitude increase of the dephasing rate has been recorded between 2 and 30 K by using accumulated photon echo technique.[12] Also, the overall exciton lifetime as measured by

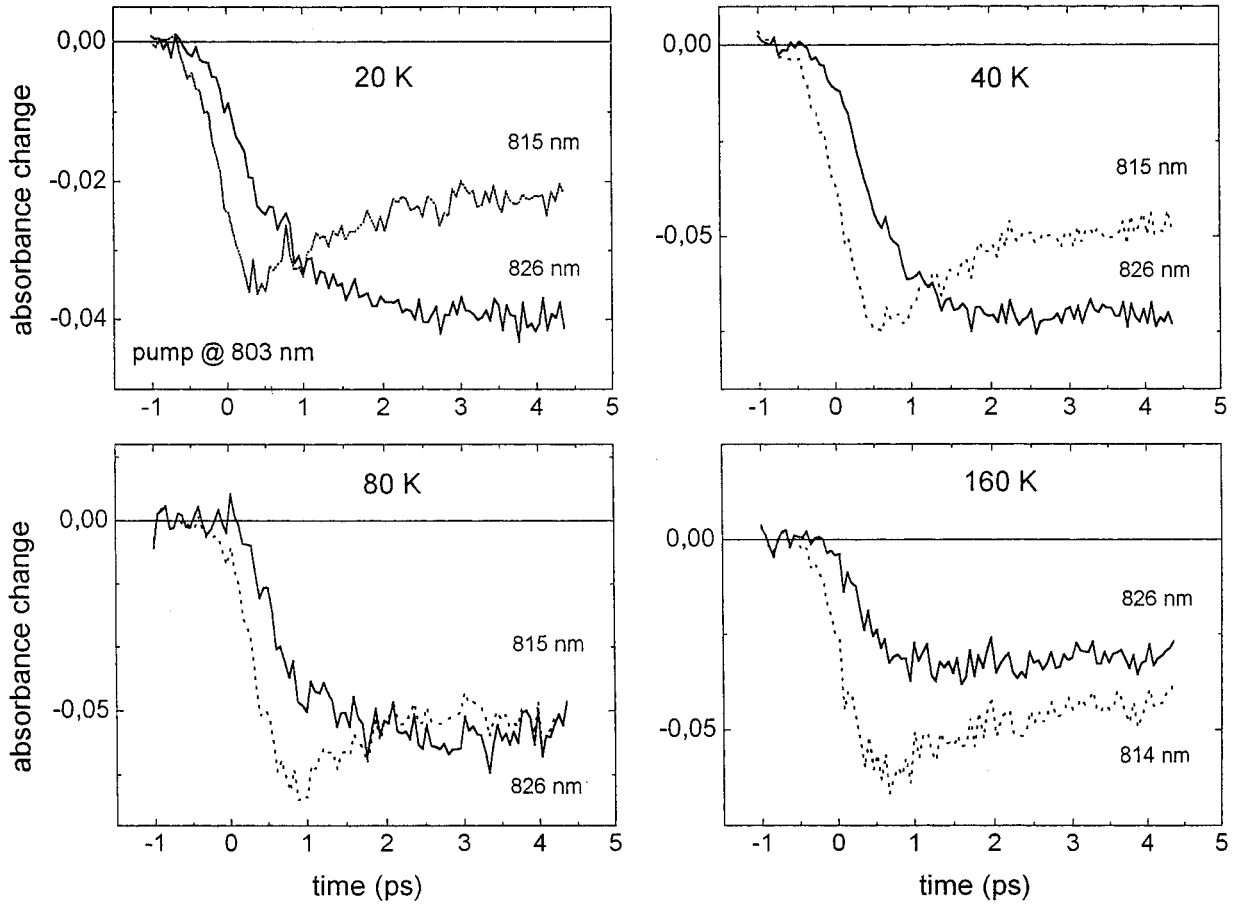

Figure 9. Absorbance kinetics at different temperatures recorded at 815 and 826 nm. Excitation is at 803 nm.

time-resolved spontaneous emission decay becomes much shorter at elevated temperatures.[6,15]

3.2. Picosecond Fluorescence Emission Data. The fluorescence emission kinetics at 805 nm excitation at 6 K are shown in Figure 10. The kinetics is not single-exponential and can be fitted only by a sum of at least three decaying and one rising exponential components. The amplitude of these components change at different recording wavelengths. The shortest decay constant varies between 7 ps (the instrument-limited value) and 60 ps, whereas the two longer ones are about 200 ps and 2 ns. The fluorescence rise time changes between 10 and 20 ps. The main effect of temperature is a speedup of the dynamics between 6 and 20 K. Further increase of temperature does not lead to the measurable dynamics changes. Above 80 K the whole emission band seems to decay as a single entity, its maximum being shifted to the blue as compared to the peak at lower temperatures.[6,15] The latter blue-shift is due to the above-mentioned equilibrium population of the higher energy exciton states.

It should be noted that the shortest emission time constants ($\leq$10 ps), deduced by using a deconvolution procedure, seem to be systematically longer when compared with the pump−probe data. This may happen if the instrument response function used for deconvolution is narrower than the proper one. In practice, evaluation of the real instrument response function is by no means a trivial problem. Even if, like in our case, resonant scattering of excitation pulses from the sample is used for that purpose, the actual instrument response function at recording wavelengths may still be different because of variant absorption conditions. However, as our experience shows, this is about the best strategy one can apply for this kind of experiment.

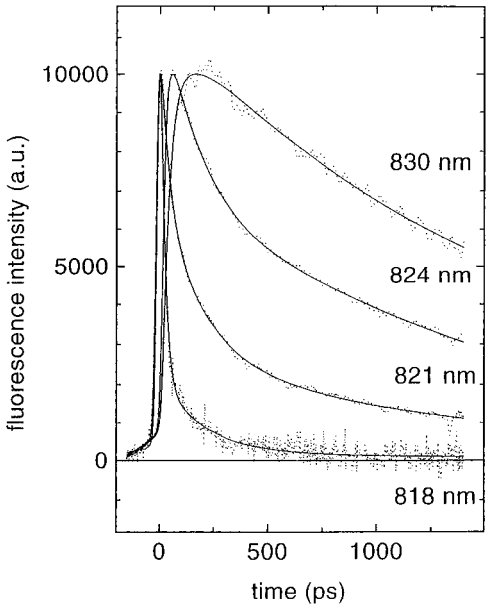

Figure 10. Normalized fluorescence emission kinetics (dots) measured at different indicated recording wavelengths (recording bandwidth 2 nm) together with the fitting functions (solid curves). Excitation is at 805 nm with laser pulses of 4 nm bandwidth, temperature is 6 K. The fitting function (see text) parameters are as follows. For recording at 818 nm: $\tau_1 = 17$ ps (amplitude 1.00), $\tau_2 = 204$ ps (0.03), and $\tau_3 = 1850$ ps (0.01). For 821 nm: $\tau_1 = 45$ ps (3.16), $\tau_2 = 205$ ps (1.57), $\tau_3 = 1920$ ps (1.00), and $\tau_4 = 8$ ps (−1.00). For 824 nm: $\tau_2 = 165$ ps (0.74), $\tau_3 = 1730$ ps (1.00), and $\tau_4 = 9$ ps (−1.00). For 830 nm: $\tau_3 = 2040$ ps (1.00) and $\tau_4 = 29$ ps (−1.00).

The transient fluorescence emission spectra were built as described in the experimental section and the result at 6 K is

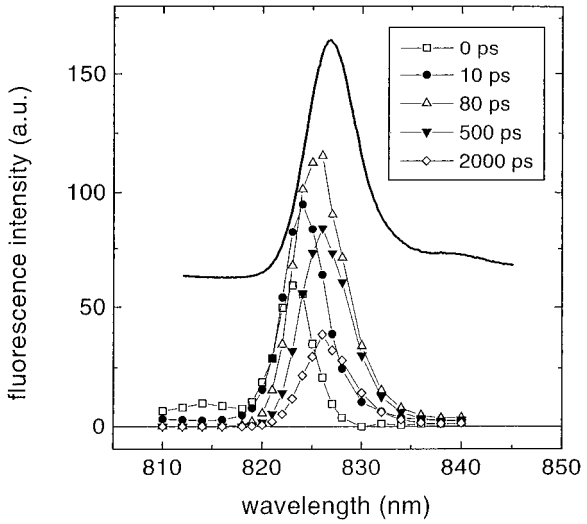

Figure 11. Transient fluorescence emission spectra at different picosecond delay times (points). The spectra are constructed as described in the experimental section. For comparison, the steady-state fluorescence spectrum is shown (thick solid line). Excitation is at 805 nm; temperature is 6 K.

presented in Figure 11. For comparison, the steady-state emission spectrum is also drawn in the upper part of Figure 11.

As seen, the TRS at short times are blue-shifted compared to the steady-state spectrum. At "zero" delay, there is an appreciable intensity in the anti-Stokes spectral band at around 815 nm, revealing initial nonequilibrium population of excitons in this region. At the same time, there is a much stronger band peaking at 823 nm. This means, in full consistency with the pump−probe data, that the population relaxation within the exciton band is very fast and that a major relaxation has already taken place during a few picosecond long excitation pulse. It is important to note that the 823 nm band is shifted by about 4 nm to the blue compared to the maximum of the steady-state emission spectrum. While the 815 nm emission band disappears completely in about 10 ps, the 823 nm band shifts toward longer wavelengths, grows in strength, and broadens. These changes last about 80 ps when both the peak position of the TRS and its width acquire nearly the same value as they have in the steady-state spectrum. Later the amplitude of the TRS begins to decline.

To this end, no physical significance is attached to the exponential kinetic components described. This functional form has been used for computational convenience only. However, let us make sure that the observed spectral evolution is not a result of trivial local heating of the BChl aggregate by excess energy provided to the excitation pulse and subsequent slow cooling due to a weak coupling to the protein matrix. Indeed, if the rate of energy dissipation to the surrounding medium is slower than the rate of heat production within the aggregate, the local temperature may increase.[19,24] The elevated temperature would manifest itself in a slight blue-shift of the 827 nm emission peak, band broadening, and most importantly, in emergence of a new anti-Stokes exciton emission peaks (see refs 6 and 25). This makes the shape of the emission spectrum a very sensitive detector of internal temperature in the FMO protein. In Figure 12, the transient emission spectrum at 10 ps delay, deduced from the emission kinetics measured at 6 K, is compared with the steady-state emission spectra at 6 and 80 K. Except a blue-shift, the shape of the TRS resembles the equilibrium spectrum at 6 K rather than the one at higher temperature. Our conclusion is that the dynamic red-shift

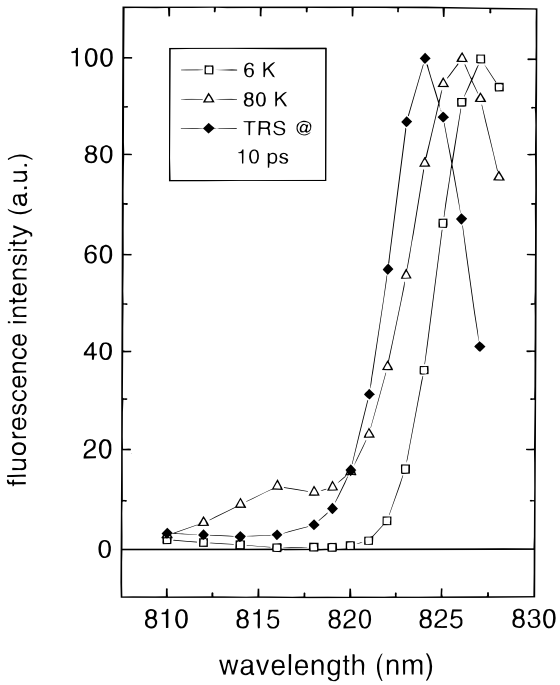

Figure 12. Transient fluorescence emission spectrum at 10 ps delay time at 6 K as compared to steady-state spectra at 6 and 80 K.

described in Figure 11 cannot primarily be a temperature effect. This conclusion is in agreement with an estimated few degrees local temperature rise based on the accepted heat capacity value of Bchl molecules (100−150 J/(mol K)[19]) and assuming that the 310 cm^{-1} excess thermal energy created during the scattering of the excitation energy (at 805 nm) to the lowest exciton state is equally distributed over all seven Bchl molecules in a protein monomer.

4. Discussion

4.1. Evaluation and Interpretation of the Pump−Probe Spectra. The first task in analyzing transient differential absorption spectra is to select its time-dependent contributions, SE and ESA. According to eq 4, the contribution of SE and ESA can be extracted by subtracting from the experimentally measured $\Delta OD(\lambda,t)$ spectrum the part due to GB:

$$\Delta OD(\lambda,t) + \sigma_{GB}(\lambda)\, n(t)d = [\sigma_{ESA}(\lambda,t) - \sigma_{SE}(\lambda,t)]n(t)d \quad (5)$$

Only processes initiating from the excited electronic state contribute now to the right-hand part of eq 5.

A major difficulty with this procedure is a correct scaling of the ΔOD and $\sigma_{GB}\, n(t)d$ terms. Here, a rough scaling has been obtained according to the following procedure. At sufficiently long delays compared to the interexciton relaxation time (e.g., at 6 ps past excitation) the spectra have been assumed to be in thermal equilibrium. In equilibrium the SE spectrum can be simulated from the known steady-state emission spectrum.[18] The amplitude of the GB spectrum relative to the ΔOD spectrum has been adjusted by combining the SE and GB spectra with about equal amplitudes (discarding about 1.5 nm Stokes shift between them). We also assumed, in agreement with available exciton calculations,[14,22] that the contribution of ESA to the lowest energy bleaching band is relatively weak.

Figure 13 demonstrates the outcome based on the above procedure at different probe delay times past excitation at 803 nm (note again, as in Figure 2, that delay times have been measured relative to the arbitrary time "zero"). By analyzing Figure 13, the following conclusions, relevant to the situation at low temperatures, can be drawn:

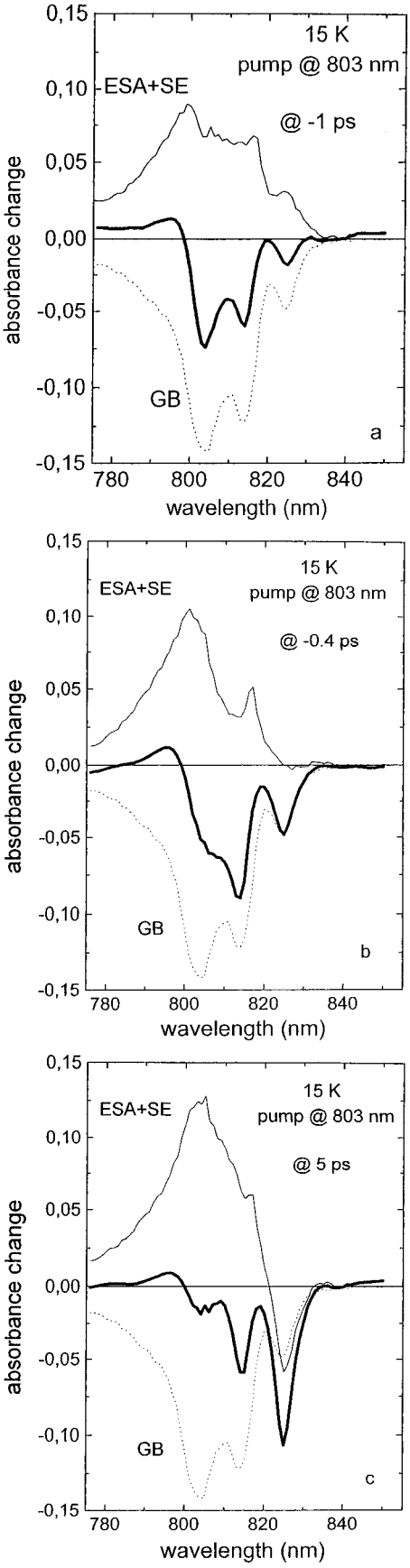

Figure 13. Result of decomposition of experimental pump−probe spectra (bold solid line) into its components at different probe pulse delay times: (a) −1 ps; (b) −0.4 ps; (c) 5 ps. GB (dotted line), ESA, and SE indicate the ground-state absorption, excited-state absorption, and stimulated emission spectra, respectively. Thin solid lines marks the composite ESA and SE spectrum. Note the proper time "zero" at about −1 ps. Excitation is at 803 nm, temperature is 15 K.

(i) The time evolution of the ΔOD spectrum seems to be mostly influenced by the SE contribution. Initially, only directly excited states are involved (Figure 13a). At later times (Figure 13b), lower states around 815 and 825 nm become increasingly more populated due to mixing (scattering) of exciton states by phonons. After a few picoseconds, when the interexciton relaxation is almost over, only the lowest state at 825 nm remains populated (Figure 13c). Further evolution of the ΔOD spectrum is mainly due to the excited-state population (the *n(t)* term in eq (4)).

(ii) The ESA spectrum is broad and less structured compared to the ΔOD spectrum and also to the ground-state absorption spectrum. Its maximum is located around 805 nm. The blue edge of the spectrum is outside our measurement range at 775 nm. The red edge of the spectrum seems to be at about 835 nm. A more spread ESA spectrum is expected considering a much increased number of states in the two-exciton band and one-exciton to two-exciton transitions compared to the number of one-exciton transitions. There are $N(N-1)/2$ two-exciton states and N one-exciton states in the respective band[22] (N is the number of coupled molecules).

(iii) The oscillator strength of ESA is comparable to the strength of the ground-state absorption. This is also what one should expect for the one-exciton to two-exciton transitions.[14,19,22,26,27]

Note that the above qualitative conclusions do not strongly depend on the exact scaling of the GB and ΔOD spectra.

4.2. Temperature Dependence of the Pump−Probe Spectra. As was mentioned above, the main effect of temperature on the ΔOD spectrum is its characteristic deformation due to broadening of the ground-state absorption spectrum and to increased equilibrium population of the upper exciton states (see Figure 8). However, a remarkable insensitivity of the interexciton population relaxation on temperature still awaits to be understood. A possible explanation relies on a relatively low density of FMO exciton states.

According to the recent calculations,[4] based on the structure of the FMO protein from *Prosthecochloris aestuarii*, the lowest two exciton states with appreciable oscillator strength are separated by an energy gap of 146 cm^{-1}. To the lowest order, scattering of the exciton from the upper state to the lower one is governed by the emission of a single-phonon mode of resonant frequency. The rate of this process is proportional to the factor of $1 + \eta$, where $\eta = [\exp(E/k_BT) - 1]^{-1}$ is the equilibrium number of normal modes with energy E at the system temperature T, and k_B is the Boltzmann constant. $\eta \ll 1$ at temperatures $T \leq 100$ K, if $E = 146$ cm^{-1}. This leads to $1 + \eta \approx 1$, and according to this naive picture, there should not be much change of the relaxation rate in this temperature range.

Relevant spectral calculations are so far available only for the FMO protein from *Prosthecochloris aestuarii*.[3,4,14] In FMO proteins from *Chlorobium tepidum* the energy gap between long-wavelength peaks of the ground-state absorption spectrum is less than in the spectrum of *Prosthecochloris aestuarii*. A similar correlation may exist between exciton states. If this is the case, then the weak temperature-induced acceleration of the relaxation rate observed between 20 and 80 K may be connected to a slight increase of the $1 + \eta$ term. An apparent slow-down of the decay rate at still higher temperatures may be due to temperature-activated back reactions from the relaxed exciton states. The rate of these processes is proportional to η and they start to play an increasingly more important role when $k_BT \cong E$.

4.3. Slow Pico−Nanosecond Dynamics Observed in the Emission Spectrum. In section 3.2, it has been found that both

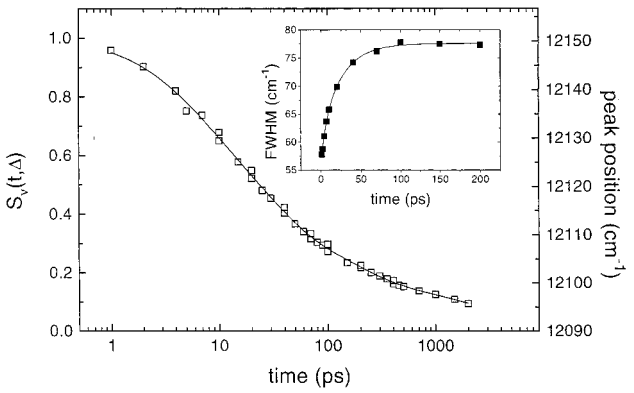

Figure 14. Relative FMO response function $S_\nu(t,\Delta)$ at 6 K, calculated as described in the text (points) together with the fitting curve (solid line). The multiexponential fitting function parameters are discussed in the text. The right-hand scale gives the FMO exciton emission band position. The insert presents the time dependence of the emission bandwidth together with the fitting curve.

the emission spectrum maximum and its width depend on time long compared to the interexciton relaxation time. In what follows, we shall discuss our results from the viewpoint of the time-dependent solute (BChl aggregate)−solvent (surrounding protein) interactions. Excitation of the BChl aggregate with a short light pulse creates a nonequilibrium initial state. Subsequent energy relaxation, in general, involves nuclear rearrangements in both the BChl and surrounding protein molecule. If the time scale of this relaxation is comparable to the exciton lifetime, the exciton emission spectrum appears to be time-dependent. The time evolution of the emission spectrum includes a red-shift of the band maximum as well as a band broadening, i.e., the effects observed in our experiment.

Within the linear response theory, the time dependence of solvation is completely characterized by the solvation energy autocorrelation function (for a recent review, see ref 28). The dynamical quantity of interest is the normalized response function, $S_\nu(t)$:

$$S_\nu(t) = [\nu(t) - \nu(\infty)]/[\nu(0) - \nu(\infty)] \qquad (6)$$

where $\nu(t)$ is the solvation free energy after a step-function solute perturbation, whereas $\nu(0)$ and $\nu(\infty)$ are the initial and equilibrated energies, respectively. Experimentally, $S_\nu(t)$ can be obtained by measuring time-resolved fluorescence emission spectra.[29] Then $\nu(t)$ is the peak energy of the spectrum at time t. It was pointed out[30] that in real experiments, only a relative response function

$$S_\nu(t,\Delta) = [\nu(t) - \nu(\infty)]/[\nu(\Delta) - \nu(\infty)] \qquad (7)$$

is measured. Here Δ is the experimental time resolution and $S_\nu(t,\Delta) = KS_\nu(t)$. The constant K denotes the fraction of the solvation dynamics occurring during the time set by the time resolution. In general, K is not known and this is a particular problem in all experimental solvation studies.

The relative response function, $S_\nu(t,\Delta)$, for the FMO protein at 6 K is plotted in Figure 14. The solvation time-scale shown extends over 4 decades, ranging from about 1 ps to almost 10 ns. During that time, the maximum of the emission spectrum shifts toward lower energy by about 55 cm^{-1}. This is a relatively minor shift compared to the typical shifts of several thousand wavenumbers in polar liquids, but perhaps, rather a substantial shift, considering the frozen state of the protein. About two-thirds of the total shift occurs within the first 50 ps past excitation. The remaining one-third needs 2 orders of magnitude longer time. To be more specific, fitting to the sum of decaying exponents reveals four time constants, each in a different decade: 5.4 ± 1.3 ps (with the amplitude of about 15 cm^{-1}), 26 ± 7 ps (23 cm^{-1}), 163 ± 58 ps (12 cm^{-1}), and 1930 ± 590 ps (7 cm^{-1}). Similar time constants have been found also at higher temperatures. Starting from about 80 K, the peak position of the emission spectrum is time independent, implying that the solvation has become very fast. One should take into account that the accuracy of these data is limited from both sides: in the low picosecond region the limit is set by the instrument, whereas in the nanosecond time domain, it is determined by the natural exciton lifetime.

The solvation response function can be deduced also from the bandwidth data.[29, 30] The insert to Figure 14 demonstrates the broadening of the exciton emission band with time at 6 K. With the band-shift alike, the initial very fast broadening is followed by a slower phase. However, differently from the shift, the equilibrium width is achieved already within 100 ps. Fitting to the sum of growing exponents gives two time constants that are very similar to the shortest ones retrieved from the shift data: 5.7 ± 3.5 ps (with the amplitude of 5 cm^{-1}) and 26 ± 5 ps (15 cm^{-1}). It is uncertain at present why the shift and width data differ at long times. We note only that the shift data are, in general, of better quality.

The nonexponential dynamical response of condensed matter to external perturbation is a universal rather than a unique phenomenon. Molecular dynamics calculations have shown[31] that the primary response can be divided into two time domains: the initial fast process, which is a single-exponential or Debye-like inertial relaxation, lasting no more than about 1 ps, and a slower process which is described by the Kohlraush−Williams−Watts stretched exponential function. Physically, this is due to heterogeneous distribution of independently (exponentially) relaxing mesoscopic regions.[32] It is therefore tempting to associate the experimental time constants with some geometrical constraints in the system as follows. (i) The 5.4 ± 1.3 ps time constant is related to the monomer exciton relaxation as described above. (ii) The 26 ± 7 ps time can be assigned to the energy transfer between monomer subunits in the FMO trimer based on similarity with the pump−probe anisotropy decay time.[13] In ref 13 the anisotropy decay time was measured between 101 and 19 K. By extrapolating to lower temperatures, one gets 12 ps at 15 K and 19.5 ps at 6 K, in close similarity to our solvation time constants at respective temperatures. The assumed energy transfer between diagonally disordered monomer exciton levels is consistent with the initial 2 nm blue-shift of the transient emission spectrum (Figure 11) compared to the ground-state absorption spectrum at 825 nm. So, only about half of the total 4 nm spectral shift at 6 K may be left over for a "proper" solvation. (iii) The "proper" solvation is characterized by 163 ± 58 and 1930 ± 590 ps time constants. They may be related, respectively, to the configurational relaxation in the protein trimer and in the whole system, including protein and its water−glycerol glass surroundings.

The given interpretation is hardly more than a speculation and leaves enough room for alternative explanations. Such as slow relaxation within the 825 nm band between closely spaced exciton states. Indeed, there is both theoretical[3,4] and experimental[11] evidence that these states do exist. The C_3 symmetry of the FMO trimer leads to two degenerate in-plane states and a nondegenerate out-of-plane state. Model simulations[3,4] offer, respectively, 2.3 and 0.4 nm spectral difference between the two lowest energy transitions. Hole-burning spectra[11] refer to the states 3.7 nm apart (at 827.1 and 824.4 nm). Our data in Figures 11 and 12 may, in principle, also be interpreted as

providing support to this hidden by spectral inhomogeneity structure. However, according to the simulations, almost all of the 825 nm transition oscillator strength is associated with either the lowest degenerate[4] or the higher energy nondegenerate[3] transition. This is a prediction that does not seem very well agree with the time-resolved emission data of Figure 11. Inclusion of exciton-vibrational coupling and spectral inhomogeneity to the model may dismiss this discrepancy. The question which remains without obvious answer in this purely excitonic approach is: why the scattering between close-lying exciton states is not only slow but also strongly nonexponential?

5. Concluding Remarks

A complex response of excitonically coupled BChl molecules in the FMO antenna protein to a short light pulse excitation has been observed at low temperatures. The response has been followed over almost 5 decades in time, from 10^{-13} to 10^{-8} s. Exciton population decay is a dominant process in the subpicosecond time domain. The relaxation rate is highest at the top of the Q_y exciton band and several times less at the band center, because fewer relaxation paths are available at lower energies. The through-band relaxation takes (as an order of magnitude) 1 ps and depends only weakly on temperature between 15 and 160 K. This insensitivity to temperature has been explained by the low density of FMO exciton states (seven in a protein monomer and fourteen in a trimer complex[3,4]) and because single-quantum vibrational processes presumably dominate the decay of exciton states.

To explain the origin of slower, pico−nanosecond, relaxation phases observed by time-resolved emission technique, a possibility has been considered that Bchl excitons trigger a solvation process in the surrounding protein and water−glycerol matrix. Early stages of this solvation are accompanied and probably hidden by the exciton relaxation. The latest stages at 6 K extend beyond the observation time window of about 2 ns. In this framework, the four distinct time constants found were related to exciton relaxation in a protein monomer ($\leq$5 ps), to energy transfer in the protein trimer between monomer subunits ($\approx$30 ps), and to a "proper" protein solvation ($\approx$ 160 ps and $\geq$2 ns). This is certainly not the first time solvation dynamics in proteins has been addressed (see, e.g., refs 33−36) but among a few performed at low temperatures (below glass transition temperature of the protein and its surrounding water−glycerol glass). Spectral diffusion at liquid helium temperatures in myoglobin and cytochrome *c* has been studied in the $\geq$10 ns time range.[37] Significant role of slow protein relaxation in tuning the charge-transfer reactions in photosynthetic reaction centers has been pointed out.[38,39] Alternatively, the 4 nm red-shift of the temporal spectra may be associated with slow relaxation between closely lying trimer exciton states.

The shape of the excited-state absorption spectrum and its oscillator strength have been roughly estimated from the analysis of the pump−probe spectrum. The spectrum peaks at around 805 nm and is less featured compared to the ground-state absorption spectrum. Both spectra have comparable strength.

Acknowledgment. The authors are grateful to W. Zhou and M. Miller for providing samples, H. van Amerongen and A. Sherman for useful discussions, and W. Struve and L. Valkunas for making available their manuscripts prior to publication (refs 13, 14, and 19). P. Kukk and M. Tars participated in the initial stage of this study. It is our pleasure to thank a referee for pointing out to us an alternative to interpret the temporal red-shift of the spectra. The work was partially performed under a NAS/NRC COBASE grant in the Arizona State University Center for the Study of Early Events in Photosynthesis (Publication No. 321). Support was also provided by the Estonian Science Foundation, Grants 247 and 2271, and by the Energy Biosciences program of the US Department of Energy, Grant DEFG03-97ER20267.

References and Notes

(1) Blankenship, R. E.; Olson, J. M.; Miller, M. Antenna Complexes from Green Photosynthetic Bacteria. In: *Anoxygenic Photosynthetic Bacteria*; Blankenship, R. E., Madigan, M. T., Bauer, C. E., Eds.; Kluwer Academic Publishers: Dordrecht, 1995; p 399.

(2) Philipson, K. D.; Sauer, K. *Biochemistry* **1972,** *11*, 1880.

(3) Lu, X.; Pearlstein, R. M. *Photochem. Photobiol.* **1993,** *57*, 86. Pearlstein, R. M. *Photosynth. Res*. **1992**, *31*, 213.

(4) Gülen, D. *J. Phys. Chem.* **1996**, *100*, 17683.

(5) Freiberg, A.; Lin, S.; Zhou, W.; Blankenship, R. E. Ultrafast Relaxation of Excitons in FMO Proteins. In: *4th Western Regional Photosynthesis Conference*; Asilomar, CA, Jan, 1995, p 15.

(6) Freiberg, A.; Kukk, P.; Tars, M.; Miller, M. Picosecond Dynamics of Excitons in Mesoscopic Pigment Aggregates of Photosynthetic Proteins. In: *Fast Elementary Processes in Chemical and Biological Systems*; Tramer, A., Ed.; American Institute of Physics Press: Woodbury, 1996; Conference Series No. 364, p 262.

(7) Freiberg, A.; Lin. S.; Zhou, W.; Blankenship, R. E. Ultrafast Inter-Exciton Relaxation Dynamics in Bacteriochlorophyll-Proteins. In: *Excitonic Processes in Condensed Matter*; Schreiber, M., Ed.; Dresden University Press: Dresden, 1996; p 275.

(8) Freiberg, A.; Lin. S.; Zhou, W.; Blankenship, R. E. Ultrafast Relaxation of Excitons in the Bacteriochlorophyll Antenna Proteins from Green Photosynthetic Bacteria. In: *Ultrafast Processes in Spectroscopy*; Svelto, O., De Silvestri, S., Denardo, G., Eds.; Plenum Press: New York, 1996.

(9) Savikhin, S; Zhou, W.; Blankenship, R; Struve, W. *Biophys. J*. **1994,** *66*, 110.

(10) Savikhin, S.; Struve, W. *Biochemistry* **1994**, *33*, 11200.

(11) Johnson, S. G.; Small, G. J. *J. Phys. Chem*. **1991**, *95*, 471.

(12) Louwe, R. J. W.; Aartsma, T. J. *J. Lumin*. **1994**, *58*, 154.

(13) Savikhin, S.; Struve, W. *Photosynth. Res*. **1996**, *48*, 271.

(14) Buck, D. R.; Savikhin, S.; Struve, W. *Biophys. J*. **1997**, *72*, 24.

(15) Zhou, W.; LoBrutto, R.; Lin, S.; Blankenship, R. E. *Photosynth. Res*. **1994**, *41*, 89.

(16) Lin, S.; Chiou, H.-C.; Kleinherenbrink, F. A. M.; Blankenship, R. *Biophys. J*. **1994,** *66***,** 437.

(17) Lin, S.; Chiou, H. C.; Blankenship, R. E. *Biochemistry* **1995**, *34*, 12761.

(18) Becker, M.; Nagarajan, V.; Parson, W. W. *J. Am. Chem. Soc*. **1991**, *113*, 6840.

(19) Gulbinas, V.; Valkunas, L.; Kuciauskas, D.; Katilius, E.; Liolia, V.; Zhou, W.; Blankenship, R. E. *J. Phys. Chem.* **1996**, *100*, 17950.

(20) Van Mourik, F.; Verwijst, R. R.; Mulder, J. M.; Van Grondelle, R. *J. Chem. Phys.* **1994**, 98, 10307; *J. Lumin*. **1992**, 53, 499.

(21) Freiberg, A.; Saari, P. *IEEE J. Quantum Electron.* **1983**, *19*, 622.

(22) Van Amerongen, H.; Struve, W. S. *J. Phys. Chem*. **1991**, *95*, 9020.

(23) Kinoshita, S.; Itoh, H.; Murakami, H.; Miyasaka, H.; Okada, T.; Mataga, M. *Chem. Phys. Lett.* **1990**, *166*, 123.

(24) Dlott, D. D. *J. Opt. Soc. Am.* **1990**, *B7*, 1638.

(25) Swarthoff, T.; Amesz, J.; Kramer, H. J.; Rijgersberg, C. *P. Isr. J. Chem*. **1981**, *21*, 332.

(26) Schelvis, J. P. M.; Aartsma, T. J. *Chem. Phys.* **1995**, *194*, 303.

(27) Novoderezhkin, V. I.; Razjivin, A. P. *Biophys. J.* **1995**, *68*, 1089.

(28) Stratt, R. M.; Maroncelli, M. *J. Phys. Chem.* **1996,** *100*, 12981.

(29) Mazurenko, Yu. T. *Opt. Spectrosc.* **1980**, *48*, 388.

(30) Ma, J.; Vanden Bout, David.; Berg, M. *J. Chem. Phys.* **1995,** *103*, 9146.

(31) Roe, R.-J. *J. Chem. Phys.* **1994**, *100*, 1610.

(32) Chamberlin, R. V. *Phys. Rev. B* **1993**, *48*, 15638.

(33) Pierce, D. W.; Boxer, S. G. *J. Phys. Chem.* **1992**, *96*, 5560.

(34) Jackson, T. A.; Lim, M.; Anfinrud, P. A. *Chem. Phys.* **1994**, *180*, 134.

(35) Riter, R. R.; Edington, M. D.; Beck, W. F. *J. Phys. Chem.* **1996,** *100*, 14198.

(36) Murakami, H.; Kushida, T. *J. Lumin.* **1994**, *58*, 172.

(37) Leeson D. T.; Wiersma, D. A. *Phys. Rev. Lett.* **1995**, *74*, 2138.

(38) Freiberg, A.; Timpmann, K.; Moskalenko, A. A.; Kuznetsova, N. Yu. *Biochim. Biophys. Acta* **1994**, *1184*, 45.

(39) Woodbury, N. W. T.; Parson, W. W. *Biochim. Biophys. Acta*, **1984**, *767*, 345.